Journal of Engineering Mechanics and Machinery (2024)
Clausius Scientific Press, Canada

DOI: 10.23977/jemm.2024.090310
ISSN 2371-9133 Vol. 9 Num. 3

Study on the Mechanism of Cavitation and Pressure Pulsation in Axial Flow Pumps under Unsteady Operating Conditions

Yu Yunyun[1,a,*], Zhou Daqing[2], Sun Ying[3], Zhang Zhichao[4]

[1]*School of Air Transportation and Engineering, Nanhang Jincheng College, Nanjing, China*
[2]*College of Energy &Electrical Engineering, Hohai University, Nanjing, China*
[3]*Jinan Energy Group Education Consulting Co., Ltd, Jinan, China*
[4]*Jinan Thermal Power Group Co., Ltd. Jinan, China*
[a]*yuyunyun@nhjcxy.edu.cn*
[*]*Corresponding author*

Keywords: Axial Flow Pump, Pressure Pulsation, Cavitation Characteristics, Experimental Validation

Abstract: This paper presents a study on the cavitation and pressure pulsation mechanisms in axial flow pumps under different cavitation margin conditions. The entire flow passage of the pump is modeled and meshed, and non-steady numerical calculations are performed using CFX software. The calculations use the M-PANS (Modified Partially Averaged Navier-Stokes) turbulence model and the Zwart cavitation model. Cavitation observations and pressure pulsation monitoring were conducted in the experiments, and the results were compared with the numerical calculations to verify the reliability of the computational methods used in this study. Pressure pulsation distributions and changes were monitored at the impeller inlet and outlet, blade suction surface, and blade tip clearance, followed by pressure spectrum analysis. By analyzing the variation patterns of pressure pulsations before and after cavitation and the observed cavitation regions in the experiments, the study explores the correlation mechanism between cavitation and pressure pulsations.

1. Introduction

Axial flow pumps, as widely used fluid transportation devices, play a crucial role in industries such as power generation, petrochemicals, and water treatment. Due to their simple structure, stable operation, and large flow capacity, axial flow pumps offer significant advantages in handling high-flow, low-head fluid transportation. However, an important issue frequently encountered during the operation of axial flow pumps is cavitation[1]. Cavitation not only leads to a decline in pump performance but can also cause severe damage to the pump body and related mechanical components. Therefore, cavitation has always been one of the key research topics in pump technology.

The occurrence of cavitation is closely related to the local pressure variations of the liquid, especially under unsteady operating conditions, where the instability of fluid flow makes the pressure fluctuations inside the pump more complex. Under these conditions, cavitation and pressure

pulsations often interact, and the correlation mechanism between them is crucial for the stability and long-term operation of the pump[2]. Pressure pulsations are periodic pressure fluctuations caused by flow instabilities, interactions between the impeller and the fluid, as well as mechanical vibrations. Particularly when cavitation occurs, pressure pulsations often intensify, subsequently affecting the pump's performance and operational safety[3]. Therefore, studying the correlation mechanism between cavitation and pressure pulsations in axial flow pumps under unsteady conditions is of great significance for improving pump design optimization, extending equipment lifespan, and enhancing operational efficiency.

In recent years, scholars both domestically and internationally have conducted in-depth research on two key issues in pump operation: cavitation and pressure pulsations. Their interaction has a profound impact on pump performance and stability. Le et al. studied the relationship between cavitation and pressure pulsations in axial flow pumps under unsteady operating conditions. Through a combination of numerical simulation and experimental methods, they found that the periodic variation of cavitation and pressure pulsations mutually influence each other to some extent, especially in the pump inlet and impeller regions, where pressure fluctuations intensify the generation and collapse of bubbles[4]. Liu et al. conducted experimental studies showing a significant correlation between the intensity of pressure pulsations and the severity of cavitation. Under high-flow conditions, pressure pulsations are typically larger, and cavitation is more pronounced. Their study also found that the occurrence of cavitation increases both the frequency and amplitude of pressure pulsations, thereby affecting pump performance and stability[5]. Jiang et al. conducted cavitation and pressure pulsation monitoring experiments on an axial flow pump test rig and validated the exacerbating effect of cavitation on pressure pulsations by combining experimental results with numerical simulations. The experimental results indicated that when the pump enters cavitation, the amplitude of pressure fluctuations increases, and the low-frequency part of the pressure spectrum becomes more prominent[6].

This study adopts the M-PANS turbulence model for numerical calculations. This model utilizes CFX software's secondary development technology to dynamically define parameters in the standard k-ε turbulence model, allowing for real-time correction based on local grid conditions and turbulence length scales. This results in higher accuracy and reliability in the numerical calculations of cavitation and pressure pulsations in the full flow path of the axial flow pump.

2. Numerical Calculation Theory and Methods

2.1 Basic Governing Equations

In CFD (Computational Fluid Dynamics) calculation methods, the governing equations of fluid dynamics are formed based on the principles of mass conservation, momentum conservation, and energy conservation. Under typical operating conditions of hydraulic machinery, where the flow medium is water, at normal temperature and pressure, and without considering heat exchange, it is generally assumed that the internal flow field is isothermal and incompressible. This assumption means that energy exchange is not considered, and only mass and momentum conservation laws are involved [7]. Therefore, the basic equations in this case include the continuity equation and the Navier-Stokes equations.

Continuity Equation [8]:

$$\partial u_i / \partial x_i = 0 \tag{1}$$

Navier-Stokes Equations [9]:

$$\frac{\partial}{\partial t}(\rho u_i)+\frac{\partial}{\partial x_j}(\rho u_i u_j)=-\frac{\partial p}{\partial x_i}+\frac{\partial}{\partial x_j}\left[(\mu+\mu_t)\left(\frac{\partial u_i}{\partial x_j}+\frac{\partial u_j}{\partial x_i}\right)\right] \tag{2}$$

In the equation, ρ represents the fluid density; p represents the fluid pressure; u_i, u_j represent the instantaneous velocities; μ represents the dynamic viscosity coefficient; μ_t represents the turbulent viscosity coefficient.

2.2 Turbulence Model

The turbulence model used in this paper is the M-PANS (Modified Partially Averaged Navier-Stokes) model, which is based on the standard PANS model. The CCL language is written using the secondary development technology of CFX to dynamically define the f_k value in the standard PANS model[10].

The standard PANS model is based on the k-ε model, and modifies the transport equations of k-ε by introducing the ratios of "unresolved turbulent kinetic energy to total turbulent kinetic energy (f_k)" and "unresolved dissipation rate to total dissipation rate (f_ε)" using the local time averaging method. For high Reynolds numbers, the value of f_ε is more appropriate when set to 1. The value of f_k has a significant impact on the results of the computation. When " f_k = 1", the PANS control equations revert to the RANS model; when " f_k = 0", the PANS control equations directly solve the N-S equations, which corresponds to the DNS model. As f_k increases from small to large values, the PANS model smoothly transitions from the DNS model to the RANS model. The standard PANS model selects a uniform f_k value within the computational domain and performs trial calculations to determine the appropriate value[11]. M-PANS dynamically defines the f_k value using CFX software, instantaneously defining f_k based on local grid conditions and turbulent length scales in space. This solves the problem in the standard PANS model where it is difficult to select an appropriate f_k value and where different f_k values cannot be assigned to different regions[12]. Compared to traditional Reynolds-averaged models, the M-PANS model provides higher numerical simulation accuracy in high-turbulence flow regions. Compared to direct simulation, it performs time-averaging in regions with small turbulence scales, reducing computational costs and improving the adaptability to grid sizes.

3. Numerical Simulation Setup and Experimental Equipment

3.1 Computational Domain and Mesh Generation

The research object in this paper is a vertical axial flow pump system. A three-dimensional model of the entire flow path of the axial flow pump is established, which consists of the inlet flow passage, impeller, rear guide vane body, and outlet flow passage. The axial flow pump model has a rated speed of 1367 r/min, a design flow rate of 0.375 m ³/s, an impeller diameter of 300 mm, a hub diameter of 120 mm, 4 impeller blades, and a blade tip clearance of 0.3 mm. The full flow path model is shown in Figure 1.

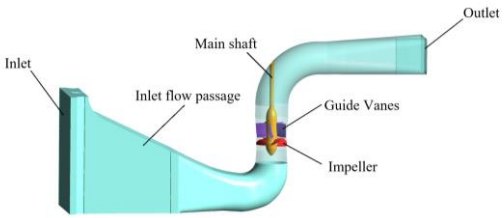

Figure 1: Axial Flow Pump Full Channel Model

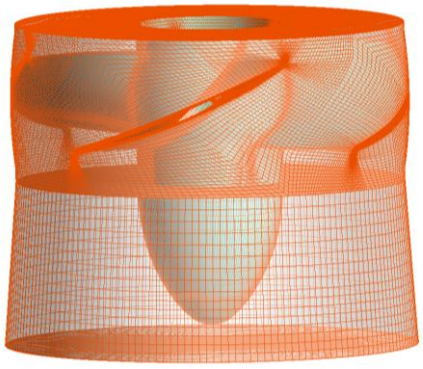

Figure 2: Impeller Body Boundary Layer Meshing

The model is meshed using hexahedral structured grids in ICEM CFD 16.0. Since the impeller and diffuser have complex structures and exhibit periodic symmetry, a periodic meshing method is employed for these two parts, where a single blade passage is meshed and then rotated and replicated. The meshes of the impeller and guide vanes are shown in Figure 2, and the mesh for the blade tip clearance is shown in Figure 3. After grid independence verification, the final mesh count for the entire flow passage is determined to be approximately 2.77 million.

3.2 Solution Method Setup

The unsteady cavitation calculation of the axial flow pump full flow passage is performed using CFX software, with the M-PANS model incorporated into the turbulence control equations. The discretization method is based on the finite volume method[13]. For the turbulence model, the convection term is solved using "high-order accuracy" and "central difference scheme." The cavitation model uses the Zwar-Gerber-Belamri model[14], and the phase transfer between the gas and liquid phases is computed using the Rayleigh-Plesset equation-based method[15]. The inlet boundary condition uses total pressure to control cavitation calculations at different Net Positive Suction Head (NPSH) values. The gas phase volume fraction at the inlet is set to 0, and the liquid phase volume fraction is set to 1. The outlet is set as a mass flow rate outlet. The fluid domain medium is set to "Water at 25 ℃" and "Water Vapor at 25 ℃". The saturated vapor pressure of water at 25 ℃ is 3175 Pa.

In the numerical calculation of unsteady flow fields, the time step can have a significant impact on the calculation results. A large time step can affect the stability of the calculation and is detrimental to accurately predicting cavitation performance, while a small time step increases the computational load[16]. Especially for simulating unsteady phenomena in pumps, too small a time step can exponentially increase the computational time cost. Therefore, in line with the requirements of this study, to improve convergence speed and computational stability, the converged steady-state results are used as the initial condition for the unsteady calculation. The initial time step is set to 0.0007315 s (corresponding to a 6 °rotation of the impeller), and once the calculation stabilizes, the time step is changed to 0.0001219 s (corresponding to a 1 °rotation of the impeller). The total computation time is 20T, and the number of iterations per step is set between 15 and 20. The rotor-stator interface is modeled using the Transient Rotor-Stator method. To monitor the instantaneous pressure changes inside the impeller, multiple monitoring points are set at the impeller inlet, outlet, on the blades, and within the impeller gap.

3.3 Test Bench Overview

The experiment was conducted on the multifunctional hydraulic machinery test rig at Hohai

University, which includes cavitation tests, pressure pulsation monitoring, and other projects. The main experimental equipment consists of the axial flow pump model, tailwater tank, pressure water tank, electromagnetic flowmeter, vacuum sensor, torque measurement device, and water supply pump. Figure 3 shows the pressure pulsation monitoring points and cavitation flashing frequency observation window of the axial flow pump.

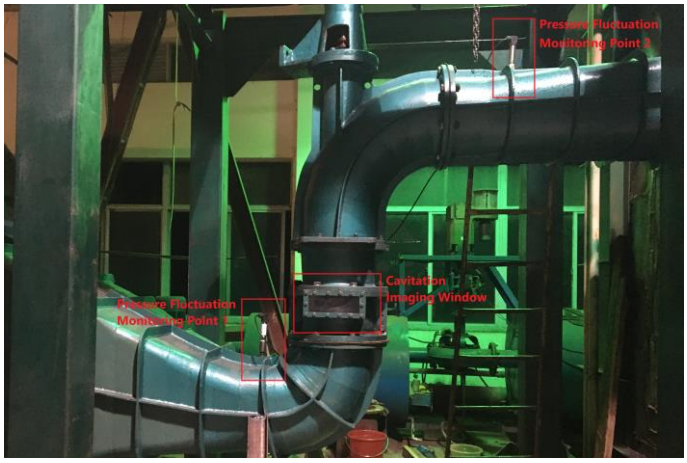

Figure 3: Configuration of Pressure Fluctuation Monitoring Points for the Axial Flow Pump Test.

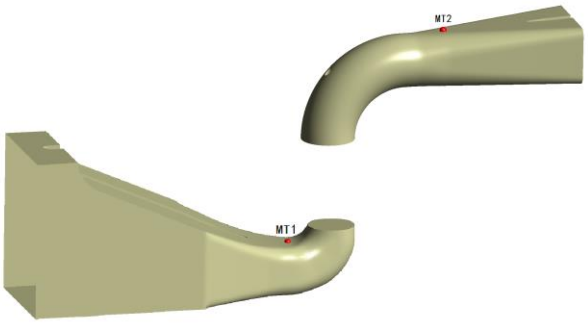

Figure 4: Setup of Verification Monitoring Points

4. Analysis of the Mechanism of the Relationship Between Cavitation and Pressure Pulsation

To verify the reliability of the pressure pulsation in the numerical simulation results, numerical simulations and experimental monitoring of the pressure pulsation in the axial flow pump under non-cavitation conditions were conducted. The layout of the numerical simulation monitoring points is shown in Figure4, where MT1 is located on the inlet flow path and MT2 is located on the outlet flow path, corresponding to the positions of the experimental monitoring points, as shown in Figure 3.

To compare and analyze the pressure data from numerical simulations and experimental monitoring, the amplitude of pressure fluctuations is selected as the comparison parameter. The pressure values at the monitoring points are subjected to Fast Fourier Transform (FFT) to obtain the amplitude and frequency of the pressure fluctuations. The dimensionalization of the amplitude is achieved using the relative amplitude method of pressure pulsations, and the formula is as follows[17]:

$$A = \frac{\Delta H}{H} \times 100\% \tag{3}$$

In the formula, H represents the head (m), and ΔH is the peak value of the pressure fluctuation amplitude (m). The comparison between numerical calculations and experimental data is shown in

Table 1.

Table 1: Comparison between Numerical Calculation and Experimental Results of Pressure Fluctuations

Monitoring Point	MT1 experimental values	MT1 numerical simulation values	MT2 experimental values	MT2 numerical simulation values
Frequency (Hz)	90.97	91.12	112.96	113.21
Relative Amplitude A	0.2526	0.2371	0.2688	0.24951

The comparison results show that the maximum peak frequency of pressure fluctuation obtained from numerical simulations is approximately the same as that from the experiments. The relative amplitude exhibits a small error, but the deviation is still within an acceptable range, and the numerical and experimental results are consistent. The reason for the error is generally that in the numerical simulation, the axial flow pump is assumed to be in an ideal environment with no external vibrations. However, in the experiment, the pressure monitoring equipment may be affected by vibrations from surrounding equipment, causing the pressure sensors to register larger amplitudes[18].

The axial pump speed is 1367 r/min, and the unit's rotational frequency is calculated to be $f=n/60=22.78$Hz. The impeller has 4 blades, and the guide vane has 5 blades. The maximum relative amplitude corresponding to the frequency at monitoring point MT1 from both the experimental and numerical simulation results is approximately 4 times the rotational frequency, which is the passing frequency of the impeller blades. The mechanism behind this is that point MT1 is located near the impeller inlet in the inlet flow passage, and its pressure fluctuation is influenced by the blade passing frequency.

The maximum relative amplitude at the monitoring point MT2 on the outlet flow passage corresponds to a frequency of 5 times the rotational frequency, indicating that this point is located after the guide vanes, and the pressure fluctuation is influenced by the passing frequency of the guide vanes. Although there is a slight discrepancy between the experimental and numerical calculation results in the main frequency, both methods capture the multiple relationship of the main frequency. This suggests that the numerical calculation method based on the M-PANS model has strong reliability in predicting pressure fluctuations.

In the cavitation test, the external characteristics of the axial flow pump and the net positive suction head (NPSH) were also measured. The cavitation test was conducted using the energy method, maintaining the design flow rate at 0.375 m^3/s. The cavitation margin was reduced by applying vacuum to the system circuit, which in turn decreased the effective cavitation margin. The head corresponding to the axial flow pump was tested at different vacuum levels, and the head and cavitation margin curves were plotted. The critical cavitation margin was determined by identifying the point where the head dropped by 2%.

The formula for the effective cavitation margin in the experimental system is as follows [19]:

$$NPSH_{av} = \frac{p_a}{\rho g} - h_v - h - \frac{p_v}{\rho g} \tag{4}$$

In the formula, h_v is the vacuum level at the vacuum gauge point, (m); h is the height difference from the impeller center to the vacuum gauge inlet, (m); $p_a/\rho g$ is the atmospheric pressure, (m); $p_v/\rho g$ is the saturated vapor pressure of water at the test water temperature, (m).

According to the above experimental method, the measured critical cavitation margin value was

5.68 m. To investigate the correlation mechanism between pressure fluctuations and cavitation, pressure fluctuation monitoring and analysis were conducted at different cavitation margin values.

4.1 Fluctuation of Cavitation Bubble Volume Fraction in the Impeller

Unsteady calculations and experiments were conducted on the axial flow pump at a cavitation margin of NPSH = 4.22m (below the critical cavitation margin). Figure 5 shows the cavitation images captured by a flash frequency meter during the experiment.

The variation of the void fraction in the impeller was monitored, and a spectral analysis was performed on the changes in the void fraction. The frequency domain graph is shown in Figure 6. From the graph, it can be observed that the maximum amplitude of the void fraction corresponds to a frequency of 22.78Hz. The main frequency coincides with the rotational frequency of the unit, meaning that the main frequency of the void fraction fluctuation is 1 times the rotational frequency.

Figure 5: Impeller Void Distribution in the Experiment

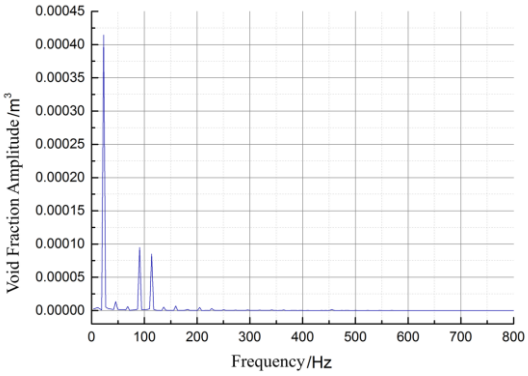

Figure 6: Frequency Domain Diagram of Cavitation Volume Fraction in the Impeller

4.2 Analysis of Pressure Fluctuations at Impeller Inlet and Outlet

The analysis focuses on the pressure fluctuations at the impeller inlet and outlet of the axial pump under different cavitation margins (NPSH = 6.81m, 4.22m). The monitoring points are shown in Figure 7, with points ZJ1, ZJ2, ZJ3, ZJ4, and ZJ5 placed on the impeller inlet side, and points ZC1, ZC2, ZC3, ZC4, and ZC5 located on the impeller outlet side.

The pressure fluctuation frequency domain graphs at the impeller inlet for each monitoring point are shown in Figure 8. These graphs display the frequency and amplitude of the pressure fluctuations at different monitoring points.

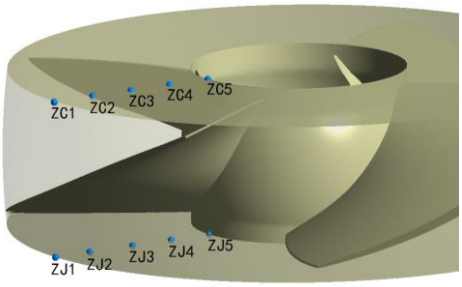

Figure 7: Impeller Inlet and Outlet Pressure Monitoring Points

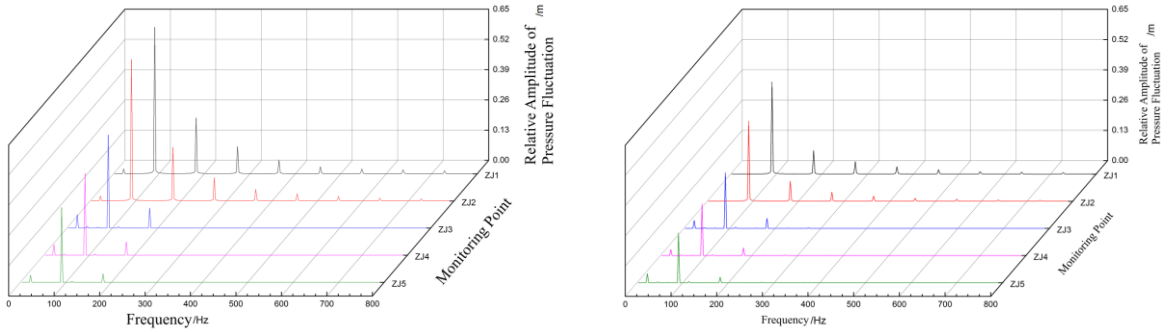

(a) NPSH=6.81m (b) NPSH=4.22m

Figure 8: Pressure Fluctuation Frequency Domain at Different Monitoring Points of Impeller Inlet

The pressure pulsation at the impeller inlet is analyzed in the frequency domain with reference to Figure 8. In Figure 8(a), when the cavitation margin is relatively high (i.e., no cavitation occurs), the main frequency at all points is four times the rotational frequency, and the secondary main frequency is eight times the rotational frequency. Since the impeller has four blades, this indicates that the pressure pulsation at the impeller inlet is primarily determined by the blade passing frequency. The relative amplitude of the main frequency increases from the hub to the tip, and at the tip, in addition to the main frequency, the amplitudes of other frequencies are also larger than those at the hub.

From Figure 8(b), it can be observed that when the cavitation margin decreases (i.e., cavitation occurs), the main frequency of the pressure pulsation at the impeller inlet remains unchanged, still being four times the rotational frequency. The primary factor affecting the pressure pulsation is still the blade passing frequency. The amplitude of the main frequency increases, with a more significant increase at points ZJ1 and ZJ2 near the tip. After cavitation occurs, the amplitude increases to approximately twice its original value. This indicates that the pressure pulsation near the tip is more significantly affected by cavitation.

The frequency spectrum analysis of the pressure pulsation at the impeller outlet is shown in the frequency domain diagram in Figure 9.

When analyzing the pressure pulsations at the impeller outlet before and after cavitation, as shown in Figure 9(a), it can be observed that when the axial flow pump operates at a higher NPSH (no cavitation), the main frequency at points ZC1 and ZC2 near the impeller rim, as well as at point ZC5 on the hub, is 92 Hz, which corresponds to 4 times the rotational frequency. This indicates that the pressure pulsations at these points are primarily influenced by the blade passing frequency of the impeller. In contrast, for points ZC3 and ZC4, located in the middle of the impeller blades, the main frequency is 115 Hz, corresponding to 5 times the rotational frequency. This suggests that the pressure pulsations at these points are mainly influenced by the guide vane passing frequency.

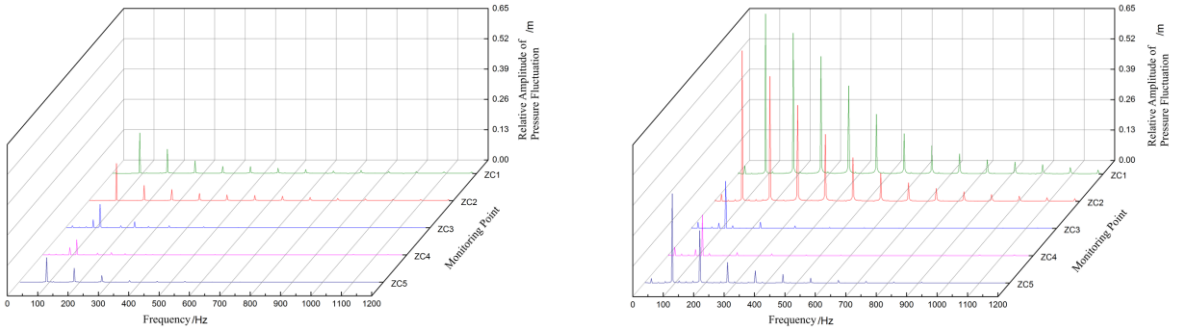

(a) NPSH=6.81m (b) NPSH=4.22m

Figure 9: Pressure Fluctuation Frequency Domain Diagram at Different Monitoring Points on the Impeller Outlet

As shown in Figure 9(b), when the axial flow pump experiences severe cavitation, the main frequency of the pressure pulsations at all points at the impeller outlet remains unchanged, but the relative amplitude undergoes a significant change. Both the main frequency and the amplitudes of other harmonic frequencies increase substantially, especially at points ZC1 and ZC2 near the impeller rim. During severe cavitation, the relative amplitude of the main frequency is about four times that of the amplitude observed when no cavitation occurs. As a result, the pressure pulsations become significantly stronger.

Comparing Figures 8 and 9, it can be seen that while the effects of severe cavitation on the pressure pulsations at both the impeller inlet and outlet exhibit similar trends, the changes in the impeller outlet pressure pulsations are more pronounced, with a greater increase in relative amplitude. This is likely due to the increased distribution of cavitation bubbles in the latter half of the blade passage.

4.3 Suction Surface Pressure Fluctuation Analysis

Since the cavitation within the impeller is primarily distributed on the suction surface of the blades, twelve pressure monitoring points were set on the suction surface. Among these, points MZ1, MZ2, MZ3, and MZ4 are located near the leading edge of the blades, while points MZ5, MZ6, MZ7, and MZ8 are near the trailing edge. The arrangement of these monitoring points is shown in Figure 10. The twelve monitoring points on the suction surface were divided into three groups: those near the leading edge, the middle of the blade, and those near the trailing edge, for pressure monitoring and fluctuation analysis. To analyze the pressure fluctuations on the suction surface of the axial flow pump blades under different cavitation margins, non-steady-state calculations were performed for two conditions: one where cavitation did not occur (NPSH = 6.81 m) and one with severe cavitation (NPSH = 4.22 m). The pressure signals obtained from the monitoring points were then subjected to Fourier transformation to determine the amplitude-frequency characteristics of the pressure fluctuations under different cavitation margins.

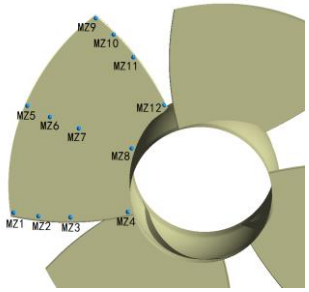

Figure 10: Layout of Pressure Monitoring Points on the Blade Suction Surface

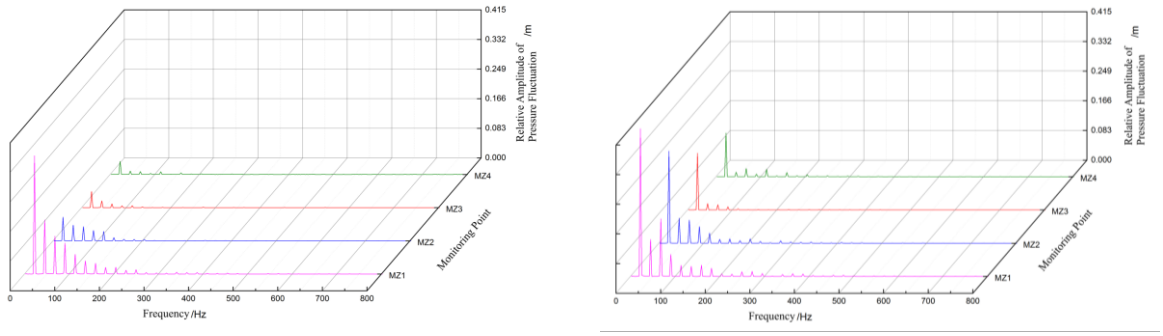

(a) NPSH=6.81m (b) NPSH=4.22m

Figure 11: Pressure Fluctuation Frequency Domain Chart at Different Monitoring Points on the Blade Suction Surface

(1) Pressure Pulsation Analysis Near the Leading Edge

Pressure monitoring was conducted at points MZ1, MZ2, MZ3, and MZ4 near the leading edge of the blade suction surface, and the pressure fluctuation signals were subjected to spectral analysis. The frequency domain diagram is shown in Figure 10.

According to Figure 11(a), the peak of the pressure fluctuation amplitude occurs at 22.78Hz, which is the same as the machine's rotational frequency. This indicates that the rotational frequency of the machine has a dominant effect on the pressure fluctuations near the leading edge of the blade suction surface. Additionally, the amplitude at each monitoring point increases radially from the hub to the tip. From the comparison of Figures 11(a) and 11(b), it can be seen that the occurrence of cavitation does not change the main frequency of pressure fluctuations at each point, which remains the same as the unit's rotational frequency. However, the peak value of the main frequency of pressure fluctuations at each point changes. Since the main frequency of the variation in the bubble volume fraction is the same as the rotational frequency, the amplitude of the main frequency increases after cavitation occurs. Combining this with the cavitation near the blade in Figure 5, it can be concluded that the collapse of bubbles has a significant impact on the pressure fluctuations.

(2) Blade Midsection Pressure Fluctuation Analysis

Pressure monitoring was conducted at points MZ5, MZ6, MZ7, and MZ8 in the middle section of the blade's suction surface, and the pressure fluctuation signals were subjected to spectral analysis. The frequency domain plots are shown in Figure 12.

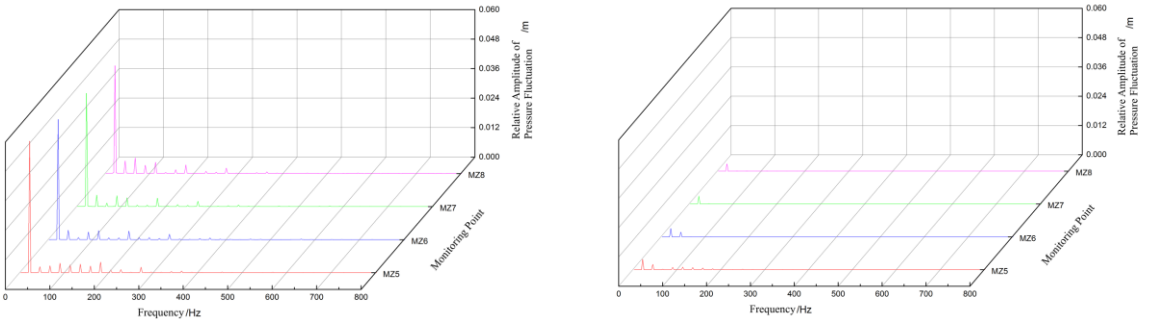

(a) NPSH=6.81m (b) NPSH=4.22m

Figure 12: Frequency Domain Diagram of Pressure Fluctuations at Different Monitoring Points on the Blade Suction Surface

From Figure 12(a), it can be observed that when no cavitation occurs, the main frequency of the pressure fluctuation in the middle of the blade suction surface is the same as the pump's rotational frequency, indicating that the pump's rotational frequency is the primary factor influencing the

pressure fluctuation at this location. However, in Figure 12(b), after cavitation occurs, although the main frequency of the pressure fluctuation remains the same, the relative amplitude significantly decreases and tends toward zero. Based on the cavitation distribution shown in Figure 5, it can be inferred that the points MZ5, MZ6, MZ7, and MZ8 on the suction surface are within the cavitation zone. Despite some fluctuations, the pressure at these points remains consistently lower than the vaporization pressure of the water, leading to a very small relative amplitude of the pressure fluctuation in these areas.

(3) Analysis of Pressure Fluctuations Near the Blade Outlet

Pressure monitoring was conducted at points MZ9, MZ10, MZ11, and MZ12, which are located near the outlet of the blade suction surface. The pressure fluctuation signals were then analyzed in the frequency domain, and the frequency domain chart is shown in Figure 13.

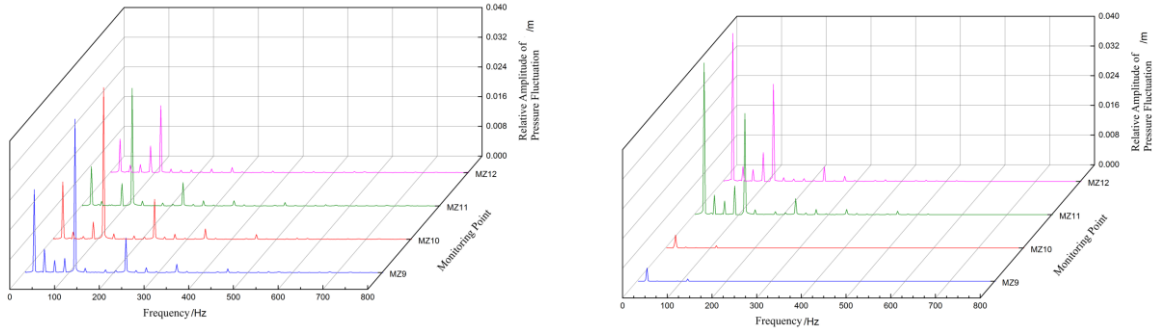

(a) NPSH=6.81m (b) NPSH=4.22m

Figure 13: Frequency Domain Diagram of Pressure Fluctuations at Different Monitoring Points on the Blade Suction Surface

According to Figure 13(a), when the pump is not cavitating, the main frequency of the pressure fluctuations near the blade suction surface outlet is 114 Hz, which is 5 times the rotational frequency. This is because the outlet of the blade is close to the guide vanes, and the dynamic-static interference between the rotating impeller and the stationary guide vanes causes the passage frequency of the guide vanes to have the main influence on the pressure fluctuations.

According to Figure 13(b), when severe cavitation occurs in the pump, it has a significant impact on the pressure fluctuations near the blade suction surface outlet. The main frequency of pressure fluctuations at each point changes from 5 times the rotational frequency to 1 time the rotational frequency, which corresponds to the main frequency of the cavitation bubble volume fraction fluctuations. This indicates that, during severe cavitation, the frequency of bubble changes has a greater influence on pressure fluctuations compared to the dynamic-static interference effect. The amplitude of the pressure fluctuations also changes: the main frequency amplitude at points MZ11 and MZ12, which are closer to the hub, increases. As shown in Figure 7, these two points are located in the boundary region with the cavitation bubble, and the collapse of the cavitation bubbles has a significant effect on their pressure, leading to a noticeable increase in the 1x rotational frequency amplitude. The pressure fluctuations near the blade tip at points MZ11 and MZ12 are weaker, with only small fluctuations at the main frequency. As seen in Figure 7, these two points are always within the cavitation bubbles, resulting in a smaller relative amplitude of pressure fluctuations.

The analysis of pressure fluctuations at the blade suction surface near the inlet, middle, and outlet regions reveals that cavitation significantly impacts pressure fluctuations. Near the inlet edge, the main frequency of pressure fluctuations remains unchanged, but the amplitude increases. At the middle of the blade, the main frequency remains the same, but the amplitude decreases and tends toward zero. Near the outlet edge, the main frequency shifts from the guide vane passing frequency to the cavitation collapse frequency. The amplitude near the hub increases, while the amplitude near

the tip decreases and tends toward zero.

4.4 Pressure Fluctuation Analysis in the Tip Clearance

Pressure fluctuation monitoring points were set in the tip clearance, as shown in Figure 14. The pressure at each monitoring point was analyzed using a frequency spectrum, and the pressure fluctuation frequency-domain diagram is shown in Figure 15.

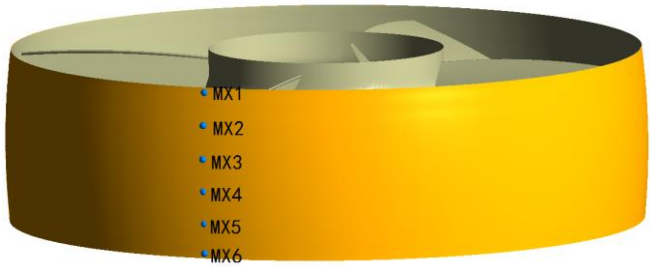

Figure 14: Layout of Pressure Monitoring Points in the Tip Clearance.

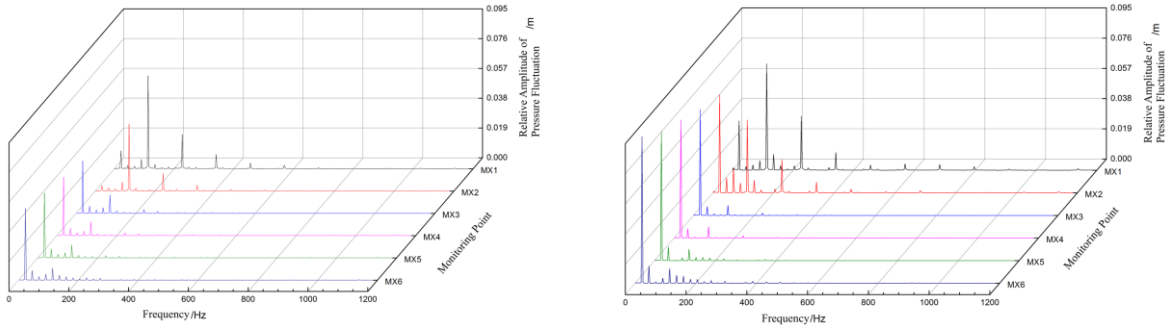

(a)NPSH=6.81m (b) NPSH=4.22m

Figure 15: Pressure Fluctuation Frequency Domain Diagram of Different Monitoring Points in the Tip Clearance

From Figure 15, it can be observed that the occurrence of cavitation has a certain impact on the pressure fluctuations within the tip clearance, causing changes in both the main frequency and amplitude of the monitoring points. In Figure 15(a), the main frequency of monitoring points MX1 and MX2 is 5 times the rotational frequency, which is mainly influenced by the passage frequency of the guide vanes, as these points are located near the impeller outlet. On the other hand, points MX3, MX4, MX5, and MX6, located further away from the guide vanes within the clearance, show a main frequency of 1 times the rotational frequency, where the impeller rotation frequency dominates the pressure fluctuations.

From Figure 15(b), it is evident that cavitation within the impeller increases the pressure fluctuation amplitude at all monitoring points within the clearance, with the greatest increase observed at points near the impeller inlet. The main frequency of point MX1 remains at 5 times the rotational frequency, indicating that the primary factor influencing the pressure fluctuations at this location is still the passage frequency of the guide vanes. However, the main frequency of point MX2 shifts from 5 times the rotational frequency to 1 times the rotational frequency, aligning with the frequency of cavitation volume fraction fluctuations. Comparing this with Figure 5, it can be seen that point MX2 is located near the region with severe cavitation at the suction side of the blade, where the influence of the passage frequency of the guide vanes is smaller than the influence of the cavitation-induced frequency changes.

From the above analysis, it can be concluded that under non-cavitation conditions, the pressure

pulsation main frequency in the clearance is influenced by the rotor rotation and the blade passing frequency. Under cavitation conditions, the main frequency and amplitude near the blade outlet change, being determined by the cavitation collapse frequency. For the remaining points in the clearance, although the main frequency does not change, the amplitude still increases, indicating that cavitation affects both the main frequency and amplitude of the pressure pulsation in the clearance.

5. Conclusions

This article performs unsteady calculations of an axial flow pump to investigate the mechanism of cavitation and pressure pulsation correlation. The reliability of pressure pulsation numerical calculations is verified through experiments, and pressure pulsations at the impeller inlet and outlet, blade suction surface, and blade tip clearance are monitored in the calculations. The main points of the study are as follows:

(1) The numerical simulation results are compared with experimental results, confirming that the computational method used in this paper has strong reliability in predicting pressure pulsations. The cavitation within the impeller is photographed, and the variation in cavitation volume fraction is monitored. The main frequency of cavitation volume fraction pulsation is found to be equal to the unit's rotational frequency.

(2) The pressure pulsations at the impeller inlet and outlet are analyzed. The main frequency of pressure pulsations at the impeller inlet and outlet remains unchanged before and after cavitation, but the amplitude increases. Notably, the pressure pulsation amplitude at the impeller outlet edge changes more significantly because more cavitation bubbles are distributed in the latter half of the impeller.

(3) The pressure pulsations on the blade suction surface are analyzed. The main frequency of pressure pulsations at the suction surface leading edge remains unchanged before and after cavitation, but the amplitude increases. The pressure pulsations in the middle area of the suction surface weaken after cavitation, reducing to near zero. The main frequency of pressure pulsations near the suction surface trailing edge changes from the guide vane passing frequency to the cavitation volume fraction pulsation main frequency.

(4) The pressure pulsations in the blade tip clearance are analyzed. The main frequency of pressure pulsations at the point near the impeller outlet in the clearance is 5 times the rotational frequency before cavitation. After cavitation, the main frequency changes to match the cavitation volume fraction pulsation main frequency. The amplitude of pressure pulsations at other points in the clearance increases.

The research results indicate that the generation and collapse of cavitation significantly affect the amplitude and frequency of pressure pulsations, especially in regions with severe cavitation, where the main frequency of pressure pulsations coincides with the main frequency of cavitation volume fraction pulsations. Future research could incorporate more experimental data and develop real-time monitoring-based online warning systems, which would help achieve more precise control and fault prevention for axial flow pumps in practical applications. This would be of great significance for improving the performance and design of axial flow pumps.

Acknowledgements

This research is supported by the 2023 School-Level Scientific Research Fund Project of Nanhang Jincheng College, titled "Study on Wake Vortex Dissipation Characteristics under Multiple Environmental Variables during Aircraft Approach" (Project No.: XJ202310), and the National Natural Science Foundation of China (Project Nos.: 51979086).

References

[1] Xu, W., & Li, S. Experimental and numerical study on cavitation in axial flow pumps: Effects on performance and materials[J]. Journal of Hydraulic Engineering, 2020, 146(7), 04020047.

[2] Zhang, X., & Liu, F. Coupling effects of cavitation and pressure pulsations in axial flow pumps and their impact on pump performance[J]. Journal of Mechanical Science and Technology, 2021, 35(8), 3475-3484.

[3] Le, T., Nguyen, L., & Dinh, D. Investigation of cavitation and pressure pulsations in axial flow pumps under unsteady operating conditions[J]. Journal of Hydraulic Engineering, 2013, 139(12), 1325-1335.

[4] Xu, L., & Zhao, F. Study on the correlation between pressure pulsations and cavitation in axial flow pumps[J]. Journal of Mechanical Engineering Science, 2020, 234(12), 2769-2781

[5] Liu, S., Xu, M., & Zhang, Y. Experimental study on the relationship between cavitation and pressure pulsation in axial flow pumps[J]. Proceedings of the Institution of Mechanical Engineers, Part A: Journal of Power and Energy, 2016, 230(1), 57-66.

[6] Jiang, Z., Cheng, Y., & Zhang, H. Experimental and numerical investigation of cavitation-induced pressure pulsations in axial flow pumps[J]. Journal of Fluids Engineering, 2019, 141(10), 101301.

[7] Huang Biao, Wang Guoyu, Quan Xiaobo, et al. Application of the PANS model in cavitating turbulence numerical calculations [J]. Journal of Applied Mechanics, 2011, 28(4): 339-343.

[8] Jiang, H., & Liu, Y. Application of the PANS model to study the cavitation flow in an axial flow pump[J]. Journal of Fluid Engineering, 2015, 137(8), 081101.

[9] Liu, Y., Zhang, Z., & Chen, S. The performance and cavitation analysis of an axial-flow pump using the PANS model[J]. Energy, 2015, 157, 874-883.

[10] Huang R, Luo X, Ji B, et al. Turbulent flows over a backward facing step simulated using a modified Partially-Averaged Navier-Stokes model [J]. Journal of Fluids Engineering, 2017, 139(4).

[11] Zhang, L., & Wang, Y. A modified PANS model for unsteady cavitating flow simulation in axial pumps[J]. Journal of Computational Physics, 2019, 376, 54-65.

[12] Chen, S., & Zhang, X. A modified PANS approach for the simulation of unsteady flow and cavitation in turbomachinery [J]. Journal of Fluid Engineering, 2020, 142(3), 031301.

[13] Ferziger, J. H., & Perić, M. Computational Methods for Fluid Dynamics[M]. 2002

[14] Zwart, P., Gerber, A. G., & Belamri, T. A two-phase flow model for predicting cavitation dynamics. Proceedings of the 5th International Conference on Multiphase Flow (ICMF 2004), Yokohama, Japan, June 7–11.

[15] Lauterborn, W., & Kurz, T. Physics of bubble oscillations. Reports on Progress in Physics,2010, 73(10), 106501.

[16] Zhou, H., Chen, Z., & Li, X. Numerical analysis of pressure pulsations and cavitation in axial flow pumps under different operating conditions[J]. International Journal of Numerical Methods for Heat & Fluid Flow, 2019, 28(8), 1476-1489.

[17] Li, J., & Chen, L. Numerical simulations of cavitation and unsteady flow in centrifugal pumps: Sensitivity to time step size[J]. International Journal of Computational Fluid Dynamics, 2021, 34(4), 220-230.

[18] Smith, J., & Johnson, R. Numerical simulations and experimental validations of axial flow pumps: An error analysis[J]. Journal of Fluid Engineering, 2019, 141(5), 051701.

[19] Liu, J., & Tang, X. Numerical and experimental study on cavitation margin in axial-flow pumps[J]. International Journal of Fluid Machinery and Systems, 2013, 16(1), 19-28.